Pergamon

Int. J. Heat Mass Transfer. Vol. 41, No. 14, pp. 2211–2220, 1998

Printed in Great Britain
0017–9310/98 $19.00+0.00

PII: S0017–9310(97)00291–3

A numerical investigation of electroconductive heating in solid–liquid mixtures

SAEED ORANGI and SUDHIR SASTRY†

Department of Food, Agricultural, and Biological Engineering, The Ohio State University, Columbus, OH 43210, U.S.A.

and

QIONG LI

Boeing Inc., Wichita, KS 67206, U.S.A.

(*Received* 20 *December* 1996 *and in final form* 10 *September* 1997)

Abstract—A mathematical model is developed to investigate the continuous-flow sterilization of solid–liquid food mixtures by electroconductive heating. Heating rates of solid and liquid phases depend on the electrical conductivities and volume fractions of the respective phases. A thermal inversion phenomenon is predicted wherein the low electrical conductivity phase which initially heats slowest, begins to heat faster than the phase of higher electrical conductivity. Effects of fluid–solid heat transfer coefficient depends on differences in electrical conductivities of phases. When electrical conductivities are sufficiently different, poor interphase heat transfer has been shown to increase overall heating rates. © 1998 Elsevier Science Ltd. All rights reserved.

INTRODUCTION

Recent developments in electrode materials have made continuous flow electroconductive, or ohmic, heating a feasible alternative for sterilization of biomaterials. This technology has found applications in heating fluids with fouling tendencies, and also in treating solid–liquid mixtures to sterility. The general objective of sterilization is the elimination of all microbial life forms: however this is not always realistic for biomaterials which also undergo severe degradation with exposure to sterilization temperatures (above 121°C). Thus, a more realistic goal is commercial sterility, or the destruction of microorganisms of public health significance.

The accomplishment of commercial sterility requires that all parts of the solid–liquid mixture be heated to a sufficient temperature for sufficient time for the purpose. If the coldest location exists within a solid piece, the difficulty in monitoring cold-spot temperatures within continuously flowing solids necessitates mathematical model development. We focus here on solids that are of significant size, such that the ratio of solid dimensions (d) to heater tube diameter $\geqslant 0.1$.

† Author to whom correspondence should be addressed. Department of Food, Agricultural and Biological Engineering, The Ohio State University, 590 Woody Hayes Drive, Columbus, OH 43210-1057, U.S.A.

Very few investigators have developed mathematical and experimental models for ohmic heating of solid–liquid mixtures. De Alwis and Fryer [1] have presented a finite element analysis of heat transfer in static heaters, in situations involving negligible convection. Sastry and Palaniappan [2, 3] studied the influence of particle orientation during the ohmic heating of liquid–particle mixtures in static heaters. These models were subjected to experimental verification with good agreement between model and experimental results.

For continuous heaters, Sastry [4] developed a model for plug flows which predicts the fluid and solid temperatures within a continuous heater. The plug flow assumption results in a one-dimensional formulation for the electric field and fluid temperature problem, although the treatment of solids conduction was fully three-dimensional. Models developed by De Alwis and Fryer [1], and Halden *et al.* [5] apply only to a single particle, rather than multiple particles, in a fluid. Furthermore these models are not three-dimensional.

In the present study, we present a mathematical model that predicts the temperature distribution in a solid–liquid mixture. We consider both axial and radial variations of the electric field and the fluid temperature in a continuous ohmic heater. A fully three-dimensional finite-element model is used to compute the temperature within solid particles. In addition, the effect of various physical parameters on temperature distributions are studied.

NOMENCLATURE

A	area [m^2]
C_p	specific heat [kJ (kg °C)$^{-1}$]
d	particle diameter [m]
h_{fp}	fluid–solid heat transfer coefficient [W (m^2 °C)$^{-1}$]
j	flow behavior index
k	thermal conductivity [W (m °C)$^{-1}$]
K	consistency coefficient [Pa s^j]
L	length of heater tube [m]
m	temperature coefficient [°C^{-1}]
$\dot{M}$	volumetric flow rate [m^3 s^{-1}]
n	number
N	number of nodal points
Nu	Nusselt number ($h_{fp}d/k_f$)
Q_c	interphase heat transfer [W m^{-2}]
r	radial coordinate [m]
R	radius of heater tube [m]
t	time [s]
T	temperature [°C]
$\dot{u}$	energy generation [W m^{-3}]
U	overall heat transfer coefficient [W (m^2 °C)$^{-1}$]
V	voltage [V]
z	axial coordinate [m].

Greek symbols

α	thermal diffusivity [m s^{-2}]
β	area fraction function
δ	Kronecker delta
v	velocity profile [m s^{-1}]
v_f	volume fraction
ρ	density [kg m^{-3}]
σ	electrical conductivity [S m^{-1} (Siemens m^{-1})]
ϕ	basis function.

Subscripts

a	air
eff	effective
f	fluid
i, j	node indices
p	solid piece
s	surface
w	wall
0	initial.

PHYSICAL MODEL

A homogeneous solid–liquid mixture is heated ohmically as it flows through a tube surrounded by air at constant temperature. Although a great variety of designs exist, we consider here a typical embodiment of a commercial heater wherein the electric field is applied longitudinally along the flow path (Fig. 1). Electric heat is generated by imposing constant but different voltages at various points along the tube, thus creating a longitudinal voltage field. The tube is assumed to be non-conductive electrically; hence, there is no voltage flux at the tube wall. Furthermore, it is assumed that the solids are spheres of uniform shape and size, and that the mass transfer between phases is negligible.

MATHEMATICAL FORMULATION

The current continuity equation (Hayt [6]) governs the electric field, while the conservative equations of continuity, momentum and energy govern the flow and thermal fields.

The steady-state form of the current continuity equation that governs the voltage distribution is given by:

$$\nabla \cdot (\sigma \nabla V) = 0. \tag{1}$$

In general, for biomaterials undergoing ohmic heating, σ is a function of temperature, and a linear relation is suitable (Palaniappan and Sastry [7]):

$$\sigma = \sigma_0(1 + mT) \tag{2}$$

where σ_0 is the reference value and m is the temperature coefficient.

The boundary conditions are:

$$V = V_1 \quad \text{at } z = 0 \tag{3}$$

$$V = V_2 \quad \text{at } z = L \tag{4}$$

and on the axis ($r = 0$) and at the outer boundaries ($r = R$):

$$\frac{\partial V}{\partial r} = 0. \tag{5}$$

If orientation effects of solid particles are negligible (i.e. the mixture is isotropic), an effective electrical conductivity, σ_{eff}, may be defined for the mixture using the Kopelman [8] model (see Sastry and Palaniappan [3]):

$$\sigma_{eff} = \frac{\sigma_f(1 - C)}{1 - C(1 - v_{fs}^{1/3})} \tag{6}$$

$$C = v_{fs}^{2/3}\left[1 - \frac{\sigma_p}{\sigma_f}\right]. \tag{7}$$

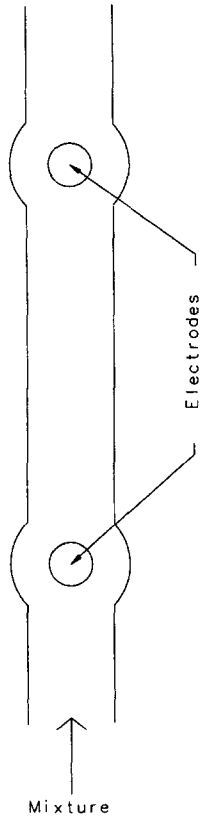

Fig. 1. Heater tube.

The above relation is derived by assuming the combined phases to consist of an equivalent circuit with a continuous phase resistance in series with two parallel resistances, each representing the continuous and dispersed (solid) phases. Note that the steady-state assumption is valid if variations in the phase properties are small, which is the assumption here.

Energy

The temperature distribution in the solid spherical particles is governed by:

$$\rho_p C_{p_p} \frac{\partial T_p}{\partial t} = \nabla \cdot (k_p \nabla T_p) + \dot{u}_p \tag{8}$$

where the energy generation term, $\dot{u}_p$, is defined by:

$$\dot{u}_p = |\nabla V|^2 \sigma_{op}(1 + m_p T_p) \tag{9}$$

where the expression $\sigma_{0p}(1+m_pT_p)$ represents the linear relation between electrical conductivity and temperature that is exhibited by many biomaterials.

Equation (8) is subject to the following initial and boundary conditions:

$$T_p = T_i, \quad \text{at } t = 0 \tag{10}$$

and at the outer surface:

$$-k_p \nabla T_p \cdot n|_s = h_{fp}(T_{ps} - T_f). \tag{11}$$

The fluid temperature is obtained from:

$$\rho_f C_{pf} \bar{v}_z v_{ff} \frac{\partial T_f}{\partial z} = \beta(v_{ff}) \nabla \cdot (k_f \nabla T_f) - n_p A_p h_{fp}(T_f - T_{ps}) + \dot{u}_f v_{ff} \tag{12}$$

where

$$\nabla^2 = \frac{\partial^2}{\partial r^2} + \frac{1}{r}\frac{\partial}{\partial r} + \frac{\partial^2}{\partial z^2} \tag{13}$$

$\dot{u}_f$ is the energy generation given by:

$$\dot{u}_f = |\nabla V|^2 \sigma_{of}(1 + m_f T_f) \tag{14}$$

and $\beta(v_{ff})$ represents the fraction of conductive heat transfer through the mixture in the fluid phase. Although the exact form of $\beta(v_{ff})$ is not known, an expression may be derived based on the fact that conduction occurs across an elemental surface. Hence $\beta(v_{ff})$ should represent the area fraction of the fluid phase. Based on the Kopelman model, the area fraction of fluid is given by:

$$\beta(v_{ff}) = 1 - (1 - v_{ff})^{2/3} \tag{15}$$

which is simplified by binomial expansion to obtain:

$$\beta(v_{ff}) = \tfrac{2}{3} v_{ff} + \mathcal{O}(v_{ff}^2). \tag{16}$$

We should note here that the particular form of this expression did not have a measurable effect on the results as the conduction term is very small relative to other terms in the fluid equation. The axial conduction term $(\partial^2/\partial z^2)$ in equation (12) is small relative to the radial conduction term by virtue of a large Peclet number, $\mathcal{O}(10^4)$, and is neglected.

The appropriate boundary conditions are as follows:

$$T_f = T_i, \quad \text{at } z = 0. \tag{17}$$

The balance between convective and conductive heat transfer on the outer surface of the tube is given by:

$$-k_f \nabla T_f \cdot n|_w = U(T_f - T_a)|_w. \tag{18}$$

Combining equations (18) and (12) provides the outer boundary condition at $(r = R)$:

$$\rho_f C_{pf} \bar{v}_z v_{ff} \frac{\partial T_f}{\partial z} = \beta(v_{ff}) \left(k_f \frac{\partial^2 T_f}{\partial r^2} - Ur(T_f - T_a) \right) - n_p A_p h_{fp}(T_f - T_{ps}) + \dot{u}_f v_{ff} \tag{19}$$

on the axis $(r = 0)$, applying the fluid equation (12) in the limit as $r \to 0$, we obtain:

$$\rho_f C_{pf} \bar{v}_z v_{ff} \frac{\partial T_f}{\partial z} = 2\beta(v_{ff}) k_f \frac{\partial^2 T_f}{\partial r^2} - n_p A_p h_{fp}(T_f - T_{ps}) + \dot{u}_f v_{ff}. \quad (20)$$

Momentum

A complete description of the flow field requires solutions of mass and momentum conservation equations that govern the fluid motion, and linear and angular momentum equations for solid pieces. In addition, the particle–fluid and particle–particle interactions must be accounted for. Since the solids in this study are not fine, but of significant dimensions, the use of fine-particle models are not useful here. Clearly, this is a formidable challenge to numerical simulation. We note that a number of multiparticle simulation approaches exist; however, these typically treat the solid particles as being fine, in effect making these point sources of momentum in the fluid equation. Other approaches, dealing with large particles, consider Stokes flow far from boundaries. Such approaches cannot easily be applied here, since the solid pieces are large and confined close to boundaries.

In most practical situations, liquids are of sufficiently high viscosity (due to the presence of large macromolecules) to ensure entrainment of solids, and prevent phase separation. This is particularly important in ensuring that end product compositions are constant. This essentially ensures that the same average velocities for both phases, and allows us to use a homogeneous flow approach. We note in passing that related studies in our laboratory using Particle Tracking Velocimetry (PTV, Zitoun [9]) have revealed that homogeneous flows occur on average; however, the fluid interstitial velocity profiles are in fact, highly complex. Indeed, significant local interphase relative velocities may exist, even though the velocities on average are essentially equal. For the present, treating the mixture as a composite non-Newtonian fluid, we express the velocity profile at each radial node in the heater tube as an average value of a fully-developed flow:

$$v_z = \left(\frac{3j+1}{j+1}\right) v_m \left[1 - \left(\frac{r}{R}\right)^{j+1_j}\right]. \quad (21)$$

NUMERICAL PROCEDURE

Discretization

Equations (8), (12), (1), and their respective initial and boundary conditions represent a set of coupled equations that are solved iteratively.

We use second-order finite-difference schemes to discretize equations (12) and (1), and their corresponding boundary conditions; the Crank–Nicholson scheme is utilized for equation (12), and a central-difference formula is used for equation (1). Second-order forward and backward difference schemes are used for inner and outer boundaries, respectively. Thus, equation (12) is reduced to the following algebraic equation:

$$\begin{aligned}
&T_{j-1}^{n+1}\left[-2\,\Delta z\alpha_f + \frac{1}{r}\Delta r\,\Delta z\alpha_f\right] \\
&+ T_{j+1}^{n+1}\left[-2\,\Delta z\alpha_f - \frac{1}{r}\Delta r\,\Delta z\alpha_f\right] \\
&+ T_j^{n+1}\left[4\,\Delta r^2 \bar{v}_{z_j} v_{ff} + 4\,\Delta z\alpha_f + 2\,\Delta r^2\,\Delta z\alpha_f h_x \right. \\
&\left. - \frac{2\,\Delta r^2\,\Delta z\alpha_f}{k_f}(|\nabla V|^2)\sigma_{of} m_f v_{ff}\right] \\
&= T_j^n\left[4\,\Delta r^2 \bar{v}_{z_j} v_{ff} - 4\,\Delta z\alpha_f - 2\,\Delta r^2\,\Delta z\alpha_f h_x \right. \\
&\left. + \frac{2\,\Delta r^2\,\Delta z\alpha_f}{k_f}(|\nabla V|^2)\sigma_{of} m_f v_{ff}\right] \\
&+ T_{j+1}^n\left[2\,\Delta z\alpha_f + \frac{1}{r}\Delta r\,\Delta z\alpha_f\right] \\
&+ T_{j-1}^n\left[2\,\Delta z\alpha_f - \frac{1}{r}\Delta r\,\Delta z\alpha_f\right] \\
&+ (T_{ps_j}^{n+1} + T_{ps_j}^n)[2\,\Delta r^2\,\Delta z\alpha_f h_x] \\
&+ \frac{4\,\Delta r^2\,\Delta z\alpha_f}{k_f}[|\nabla V|^2)\sigma_{of} v_{ff}] \qquad (22)
\end{aligned}$$

where

$$|\nabla V|^2 = \frac{(|\nabla V|^2)_j^{n+1} + (|\nabla V|^2)_j^n}{2}$$

$$\alpha_f = \frac{k_f}{\rho_f C_{pf}}$$

$$h_x = \frac{n_p A_p h_{fp}}{k_f}.$$

The algebraic equation (22) along with the inner and outer boundary conditions is solved by matrix inversion. The explicit finite-difference form of equation (1), which is obtained using a central-difference scheme, is solved by the Gauss–Seidel iteration. An approximate solution to equation (8) is constructed using Galerkin's method and the Crank–Nicholson scheme. Utilizing Galerkin three-dimensional finite-element method in space and Crank–Nicholson finite-difference scheme in time, equation (8) and its boundary conditions are reduced to a set of algebraic equations:

$$\sum_{i=1}^{N}\left[C_{ij} + \frac{\Delta t}{2}K_{ij}\right]T_i^{n+1} = \sum_{i=1}^{N}\left[C_{ij} - \frac{\Delta t}{2}K_{ij}\right]T_i^n + \frac{\Delta t}{2}[F_j^{n+1} + F_j^n] \quad \text{for } j = 1, 2, \ldots, N \quad (23)$$

where, for surface nodes:

$$C_{ij} = \frac{1}{\alpha_p}\int_v \phi_i\phi_j \,dv \tag{24}$$

$$K_{ij} = \int_v (\nabla\phi_i \cdot \nabla\phi_j)\,dv - \frac{|\nabla V|^2\sigma_{op}}{k_p} m_p \int_v \phi_i\phi_j \,dv + \frac{h_{fp}}{k_p}\int_s \phi_i\phi_j \,ds \tag{25}$$

$$F_j = \frac{|\nabla V|^2\sigma_{op}}{k_p}\int_v \phi_j \,dv + \frac{h_{fp}}{k_p} T_f(t)\int_s \phi_j \,ds \tag{26}$$

and for internal nodes:

$$C_{ij} = \frac{1}{\alpha_p}\int_v \phi_i\phi_j \,dv \tag{27}$$

$$K_{ij} = \int_v (\nabla\phi_i \cdot \nabla\phi_j)\,dv - \frac{|\nabla V|^2\sigma_{op}}{k_p} m_p \int_v \phi_i\phi_j \,dv \tag{28}$$

$$F_j = \frac{|\nabla V|^2\sigma_{op}}{k_p}\int_v \phi_j \,dv. \tag{29}$$

In the foregoing expressions, the ϕ_i's, are the basic functions, which are first-degree polynomials chosen in such a way that $\phi_i(x_j, y_j, z_j) = \delta_{ij}$.

The choice of computational methods was dictated partly by the problem, and partly by available internally written codes. The finite difference approach was preferred for the tube geometry for two reasons: better ability than finite elements to handle the parabolic thermal problem, and the regular geometry, which was not likely to change significantly. Finite elements were chosen for the solid heat transfer problem because of the easier transition to complex geometries (likely with food particles) and the availability of our own code for this purpose.

Mesh for tube geometry

The finite-difference mesh for the heater tube containing the solid–liquid mixture is as represented in Fig. 2(a). This mesh is used for both the voltage and fluid temperature equations. Mesh refinement is limited by solids size. Refinement to sub-particle sizes

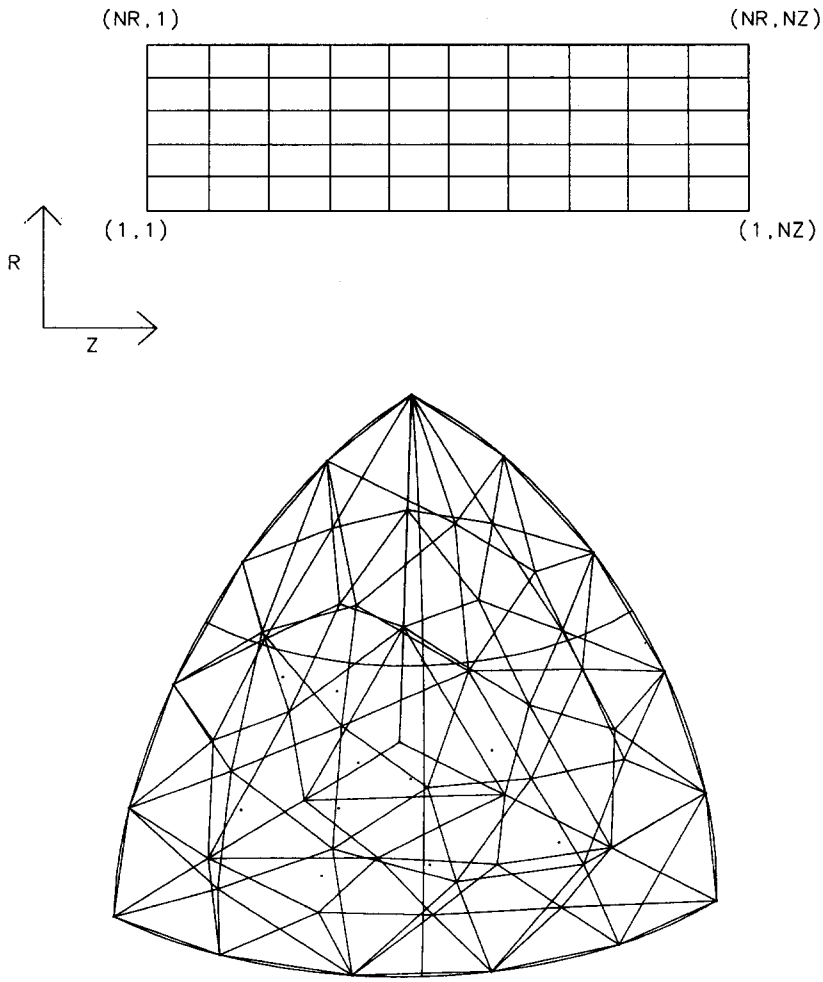

Fig. 2. (a) Finite-difference mesh for heater tube. (b) Finite-element mesh for solid particles.

will invalidate the original working equations, a common drawback of such approaches. Approaches such as ensemble-averaging may be used for multiphase flows (Lahey and Drew [10]). In this study, we used meshes that would accommodate at least one complete solid particle within an element.

Mesh for solids geometry

The finite-element mesh constructed using SDRC's I-DEAS Master series. The domain, in our case a segment of a sphere bounded by three symmetrical surfaces, namely the coordinate axis, and the outer surface, is partitioned into 173 tetrahedral elements with a total of 63 nodal points. The mesh is depicted in Fig. 2(b). Preliminary simulations revealed that temperature gradients within individual particles were not large enough to necessitate the use of non-uniform meshes.

Iteration process

Since the governing equations are coupled, suitably converged solutions are obtained iteratively. We define all physical properties, construct the nodal network, and specify initial profiles for fluid and particle temperatures. The iteration proceeds as follows: first, the voltage distribution is computed, and then the fluid and particle temperatures are obtained across the tube radius simultaneously. At each axial location the fluid temperature is computed by matrix inversion and the temperature distribution in particles are obtained at each node. An average particle-surface temperature is then computed to represent the particle temperature at each node. This process is repeated until convergence is attained. The convergence criteria requires that the maximum difference between fluid temperatures and also the particle temperatures in two successive steps be less than the convergence tolerance. It is important to note that the time steps are chosen such that successive time steps coincide with the axial location in the heater tube. In other words, the time step depends on the number of axial nodes, the dimensions of the heater tube, and the volume flow rate:

$$\Delta t = \frac{(\pi R^2)L}{\dot{M}(N_z - 1)}. \tag{30}$$

We performed a parametric study to determine the effects of various physical parameters (e.g. fluid–solid convective heat transfer coefficient, solid volume fraction, particle size, electrical conductivities of phases) on the temperature distribution in the fluid and solid particles. Table 1 contains the values of system parameters and physical properties of fluid and solid particles used in our simulations.

All computations were carried out on a Cray Y-MP supercomputer. The total computation time for a converged solution varied from a minimum of 285 s to a maximum of 600 s depending on the physical properties and system parameters. For example, higher values of σ and h_{fp} required more iterations to attain convergence. A total of 1200 nodal points, 200 in the axial and six in the radial direction, covered the tube. The convergence tolerance was set at $0.1e-4$°C.

RESULTS AND DISCUSSION

The effect of the finite-element mesh refinement is depicted in Fig. 3. Increasing the number of nodes and elements, uniformly, from 30 and 55, respectively, to 63 and 173 changed the particle temperature by 1%. A further increase to 96 nodes and 288 elements produced no discernible change in the particle temperature. The change in the fluid temperature was smaller than that in particle temperature for all cases.

Table 1. (a) System parameter values. (b) Physical properties

Parameter	Value
Length of tube	5.0 m
Tube diameter	0.10 m
V_1	0.1e+05 V
V_2	0.25e+04 V
Volumetric flow rate	$0.4e-03$ m^3 s^{-1}
Particle size	0.004 m
Solid volume fraction	0.50–0.80
Initial temperature	25°C
Overall heat transfer coefficient	20 W m^{-2} C^{-1}
Fluid-particle heat transfer coefficient	100–300 W m^{-2} C^{-1}
Flow behavior index	0.30

Property	Solid	Fluid
Electrical conductivity (reference value at 0°C)	0.1–0.2 S m^{-1}	0.2–0.6 S m^{-1}
Temperature coefficient of electrical conductivity	0.25°C^{-1}	0.02°C^{-1}
Specific heat	3.57 kJ kg^{-1} °C^{-1}	3.76 kJ kg^{-1} °C^{-1}
Thermal conductivity	0.55 W m^{-1} °C^{-1}	0.5 W m^{-1} °C^{-1}
Density	1080 kg m^{-3}	1000 kg m^{-3}

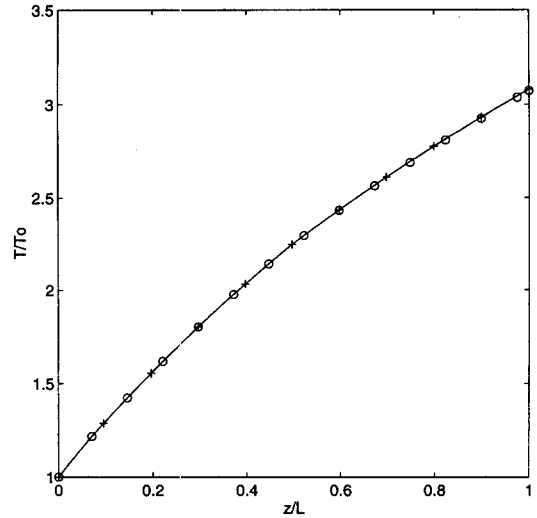

Fig. 3. Particle temperature distribution for various mesh sizes ($\sigma_{0p} = 0.1$, $\sigma_{0f} = 0.59$, $v_{fs} = 0.5$, $h_{fp} = 100$, $m_f = 0.02$, $m_p = 0.25$), ○ (55 elements), — (173 elements), +(288 elements).

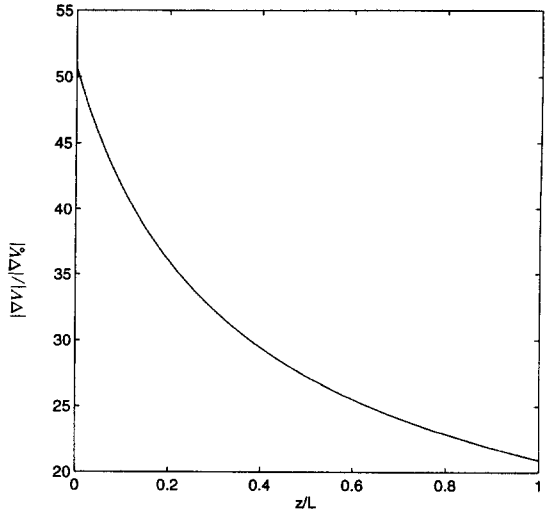

Fig. 5. Electric field distribution in the mixture ($\sigma_{0p} = 0.1$, $\sigma_{0f} = 0.59$, $v_{fs} = 0.5$, $h_{fp} = 100$, $m_f = 0.02$, $m_p = 0.25$).

The fluid and solid cold-spot temperatures, at the center line of the heater tube, are plotted as functions of axial location in Fig. 4. It is observed that the particles lag the fluid thermally nearly midway through the heater. Because of a much larger electrical conductivity, the fluid heats at a faster rate than do the particles resulting in a higher fluid temperature. However, as the temperature rises, the electrical conductivity of the particles increases rapidly due to a larger temperature coefficient value (this is typical of biomaterials). Consequently, the particles begin to lead the fluid thermally.

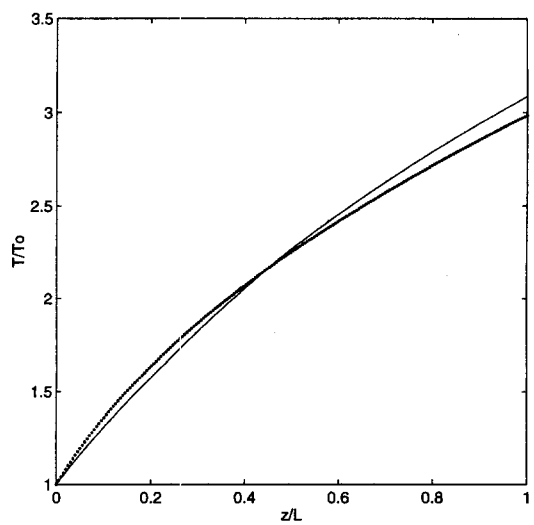

Fig. 4. Temperature distribution in the heater tube ($\sigma_{0p} = 0.1$, $\sigma_{0f} = 0.59$, $v_{fs} = 0.5$, $h_{fp} = 100$, $m_f = 0.02$, $m_p = 0.25$), — particle, ··· fluid.

The electric field distribution is shown in Fig. 5 for various radial locations. The upstream locations show large field strengths, since the mixture is coldest and least electrically conductive at these locations. As the temperature rises, the electrical conductivities increase, and the field-strength decreases.

Radial variation of heating rates in solid particles and fluid are illustrated in Figs. 6(a) and (b), respectively. As expected the heating rate increases in the direction of the outer wall of the heater where the residence time reaches its maximum.

Temperature distributions for different values of heat transfer coefficient, h_{fp}, are shown in Figs. 7(a) and (b). Two distinct patterns may be observed. When the electrical conductivities of the two phases do not differ by large amounts (Fig. 7(a)), in mixtures with larger values of h_{fp}, heat exchange between solid and liquid phases is more significant. As a result the particle and fluid temperature differences are reduced as h_{fp} increases. Figure 7(b), however, illustrates a situation where the electrical conductivities of the two phases are widely different. In such a situation, it is possible for one phase to heat sufficiently rapidly as to create a large temperature difference between it and the other phase. Under such conditions, the low h_{fp} mixture develops an increased interphase heat flux (Fig. 8) which causes the entire mixture to heat more rapidly than the mixture with a higher heat transfer coefficient. This observation has been experimentally verified in our laboratory (Khalaf and Sastry [11]).

It is noted that experimental verification for flowing conditions is not simple, since the measurement of flowing solids' temperatures is not easily possible. However, monitoring of fluid temperature and power are possible, and provide indications of overall mixture heating. Data from Khalaf and Sastry [11] showing the effect of heat transfer coefficient (varied by

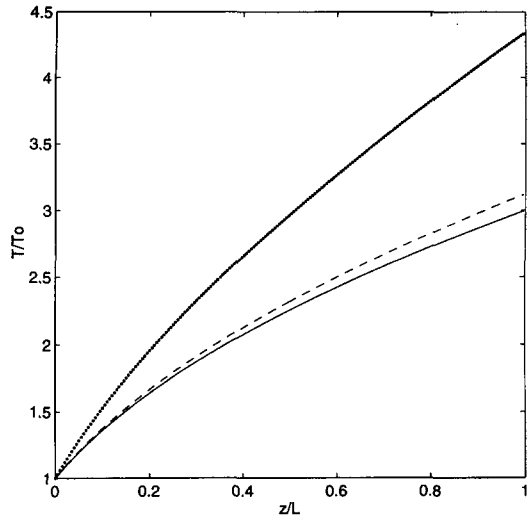

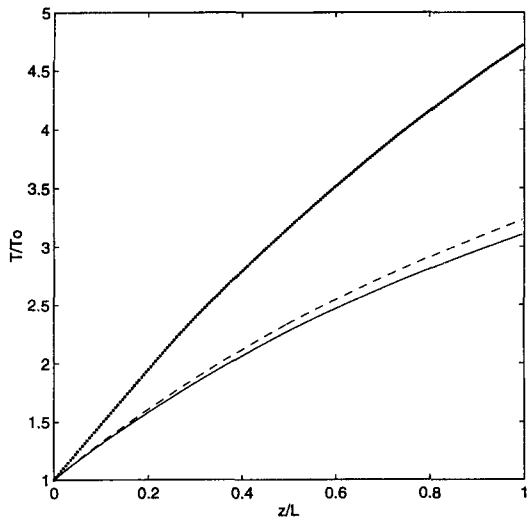

Fig. 6. Temperature distribution for various radial locations ($\sigma_{0p} = 0.1$, $\sigma_{0f} = 0.59$, $v_{fs} = 0.5$, $h_{fp} = 100$, $m_f = 0.02$, $m_p = 0.25$), — $r = 0.0$, - - - $r = R/2$, ··· $r = R$. (a) Particle. (b) Fluid.

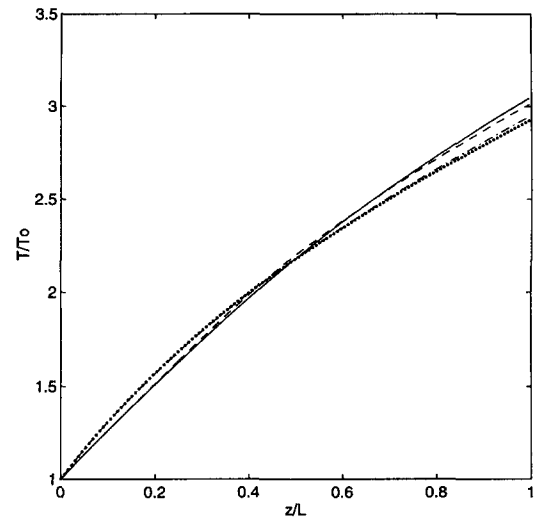

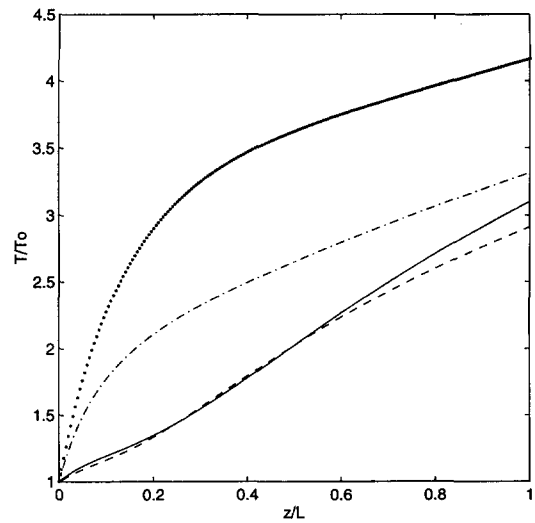

Fig. 7. Temperature distribution for various h_{fp} values ($\sigma_{0p} = 0.1$, $\sigma_{0f} = 0.59$, $v_{fs} = 0.5$), particle: — $h_{fp} = 100$, - - - $h_{fp} = 300$, fluid: ··· $h_{fp} = 100$, -·-·- $h_{fp} = 300$, (a) $m_f = 0.02$, $m_p = 0.25$, (b) $m_f = 0.1$, $m_p = 0.1$.

changing viscosity) are shown in Table 2. While the total amounts of heating are small (dictated by large electrode gaps), the increased heating rate of the higher viscosity solution is evident. Space does not permit the presentation of verification of thermal inversion (Sastry and Palaniappan [3]); the reader may refer to that paper for details.

The effect of the solid volume fraction, v_{fs}, is depicted in Fig. 9(a); an upward shift is observed in both the fluid and particle temperatures, at higher solid concentrations. The effective electrical conductivity of the mixture is increased with increasing solid concentration and rising temperatures resulting in higher heating rates. It is also noted that the thermal inversion point (the point where the solids temperature exceeds that of the fluid) occurs at a lower temperature when the volume fraction increases. This appears to be due to the larger fraction of total electrical energy intercepted by the dispersed phase as the volume fraction increases.

Results presented in Fig. 9(b) show the influence of particle size on the heating rates. As particle size is reduced, the number of particles per unit volume of the mixture, and consequently, the total solid surface area is increased. This increases the interphase convective heat exchange which causes the particle and fluid temperatures to approach each other. In addition, a small increase is observed in both the particle and fluid temperatures.

It must be noted that the model presented here is subject to simplifying assumptions regarding the fluid velocity profiles, as well as the structure of the mixture

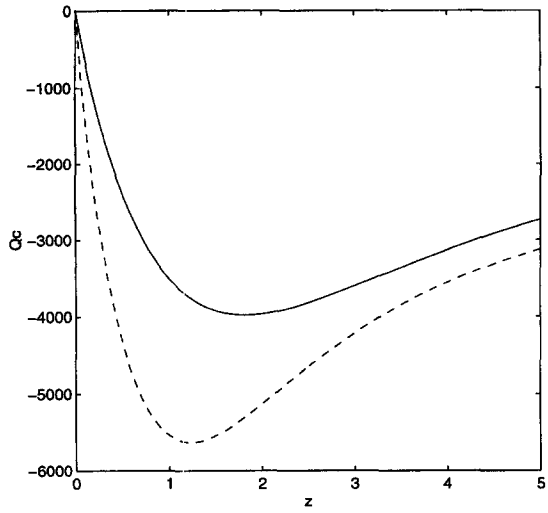

Fig. 8. Interphase heat exchange for various h_{fp} values ($\sigma_{0p} = 0.1$, $\sigma_{0f} = 0.59$, $v_{fs} = 0.5$, $m_f = 0.1$, $m_p = 0.1$), — $h_{fp} = 100$, - - - $h_{fp} = 300$.

used in determining the effective electrical conductivity. In a real flowing solid–liquid mixtures, the solid areal porosity (area fraction exposed to the current) is a complex, stochastic function, and the fluid velocity is extremely complex. These issues affect the temperature distribution function, but are not presently tractable either due to lack of information or computational limitations relative to the flow structure. These points are the subjects of ongoing model refinements.

CONCLUSIONS

The ohmic heating of solid–liquid mixtures shows potential for heating solid materials faster than the surrounding liquid medium. Heating rates depend on the electrical conductivities of the two phases. For typical values of electrical conductivity of liquid and solid phases, a thermal inversion point occurs, where the heating rate of the solid phase exceeds that of the liquid. The thermal inversion point has been found to depend on solids volume fraction. Radial location affects heating because of the low residence times associated with central tube locations. The fluid–solid heat transfer coefficient shows two distinct types of behavior. When electrical conductivities are not widely apart, the effect of increased heat transfer coefficient is simply one of reducing interphase temperature difference. However, when phase electrical conductivities differ markedly, one phase may heat significantly faster than another, and the interphase energy flux is dictated more by temperature difference than heat transfer coefficient. Particle size has a small effect on overall heat transfer.

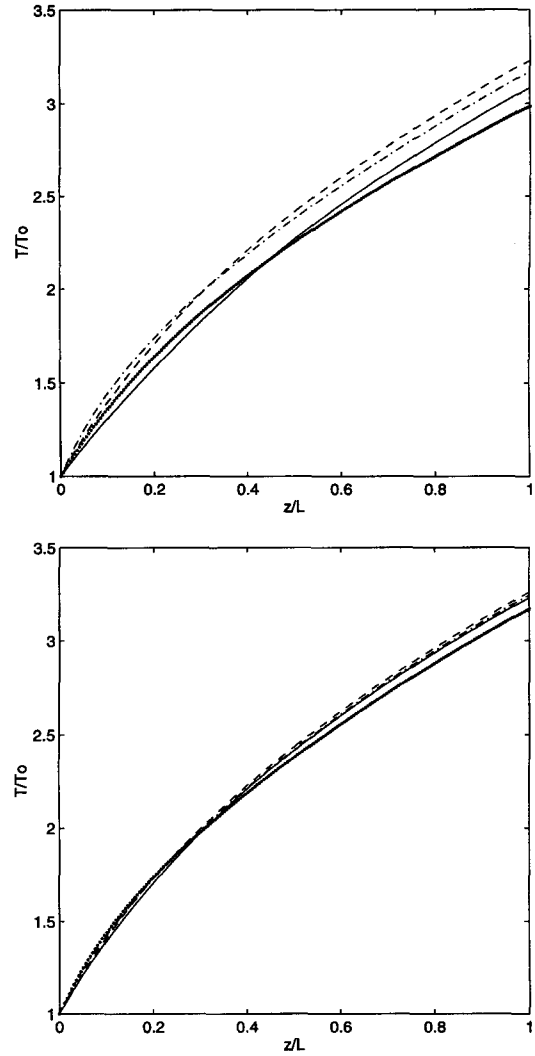

Fig. 9. Temperature distribution for various v_{fs} values and particle sizes ($\sigma_{0p} = 0.1$, $\sigma_{0f} = 0.59$, $h_{fp} = 100$, $m_f = 0.02$, $m_p = 0.25$), (a) particle: — $v_{fs} = 0.5$, - - - $v_{fs} = 0.8$, fluid: ··· $v_{fs} = 0.5$, -·-·- $v_{fs} = 0.8$, (b) particle: — $d/L = 0.0016$, - - - $d/L = 0.0004$, fluid: ··· $d/L = 0.0016$ ($v_{fs} = 0.8$), -·-·- $d/L = 0.0004$ ($v_{fs} = 0.8$).

Table 2. Comparison of continuous flow heating of 60% potato solids in sodium carboxymethyl cellulose solutions of equal electrical conductivity (data from Khalaf and Sastry [11])

	Fluid carrier	
Parameter	$K = 0.179$ Pa $s^{0.72}$	$K = 0.87$ Pa $s^{0.6}$
σ_{0f} (S m^{-1})	0.57	0.59
m_f ($°C^{-1}$)	0.04	0.039
σ_{0p} (S m^{-1})	0.1	0.1
m_p ($°C^{-1}$)	0.163	0.163
$\dot{M}$ (m^3 s^{-1})	1.7	1.7
Voltage (V)	697	697
Electrode gap (m)	0.72	0.72
Power dissipation (W)	3187	3497
Temperature rise (°C)	3.8	6.8

Acknowledgements—Salaries and research support provided in part by OARDC, The Ohio State University, and USDA-NRICGP Grant No. 93-37500-9255, and computational resources provided by the Ohio Supercomputer Center. References to commercial products and trade names are made with the understanding that no endorsement or discrimination by The Ohio State University is implied.

REFERENCES

1. De Alwis, A. A. P. and Fryer, P. J., A finite element analysis of heat generation and transfer during ohmic heating of food. *Chem. Eng. Sci.*, 1990, **45**(6), 1547–1559.
2. Sastry, S. K. and Palaniappan, S., Influence of particle orientation on the effective electrical resistance and ohmic heating rate of a liquid–particle mixture. *J. Food Proc. Eng.*, 1992a, **15**, 213–227.
3. Sastry, S. K. and Palaniappan, S., Mathematical modeling and experimental studies on ohmic heating of liquid–particle mixtures in a static heater. *J. Food Proc. Eng.*, 1992b, **15**, 213–227.
4. Sastry, S. K., A model for heating of liquid–particle mixtures in a continuous flow ohmic heater. *J. Food Proc. Eng.*, 1992, **15**, 263–278.
5. Halden, K., De Alwis, A. A. P. and Fryer, P. J., Changes in the electrical conductivities of foods during ohmic heating. *Int. J. Food Sci. Tech.*, 1990, **25**, 9–25.
6. Hayt, W. H., *Engineering Electromagnetics*, 5th edn. McGraw-Hill Book Co., New York, 1988.
7. Palaniappan, S. and Sastry, S. K., Electrical conductivity of selected solid foods during ohmic heating. *J. Food Proc. Eng.*, 1991, **14**, 221–236.
8. Kopelman, I. J., Transient heat transfer and thermal properties in food systems. Ph.D. thesis, Michigan State University, East Lansing, MI, 1966.
9. Zitoun, K. B., Continuous flow of solid–liquid mixtures during ohmic heating: fluid interstitial velocities, solid area fraction, orientation and rotation. Ph.D. thesis, The Ohio State University, Columbus, OH, 1996.
10. Lahey, Jr., R. T. and Drew, D. A., The three dimensional time- and volume-averaged conservation equations of two-phase flow. *Advances in Nucl. Sci. and Technol.*, 1988, **20**, 1–69.
11. Khalaf, W. G. and Sastry, S. K., Effect of fluid viscosity on the ohmic heating rate of solid–liquid mixtures. *J. Food Engineering*, 1996, **27**, 145–158.